

Article

# Steam Gasification of Sawdust Biochar Influenced by Chemical Speciation of Alkali and Alkaline Earth Metallic Species

Dongdong Feng, Yijun Zhao \*, Yu Zhang, Shaozeng Sun and Jianmin Gao

School of Energy Science and Engineering, Harbin Institute of Technology, Harbin 150001, China; 08031175@163.com (D.F.); 14B902024@hit.edu.cn (Y.Z.); sunsz@hit.edu.cn (S.S.); yagjm@hit.edu.cn (J.G.)

\* Correspondence: zhaoyijun@hit.edu.cn; Tel.: +86-451-8641-3231; Fax: +86-451-8641-2528

Received: 8 December 2017; Accepted: 8 January 2018; Published: 15 January 2018

**Abstract:** The effect of chemical speciation ( $\text{H}_2\text{O}/\text{NH}_4\text{Ac}/\text{HCl}$ -soluble and insoluble) of alkali and alkaline earth metallic species on the steam gasification of sawdust biochar was investigated in a lab-scale, fixed-bed reactor, with the method of chemical fractionation analysis. The changes in biochar structures and the evolution of biochar reactivity are discussed, with a focus on the contributions of the chemical speciation of alkali and alkaline earth metallic species (AAEMs) on the steam gasification of biochar. The results indicate that  $\text{H}_2\text{O}/\text{NH}_4\text{Ac}/\text{HCl}$ -soluble AAEMs have a significant effect on biochar gasification rates. The release of K occurs mainly in the form of inorganic salts and hydrated ions, while that of Ca occurs mainly as organic ones. The  $\text{sp}^3$ -rich or  $\text{sp}^2$ - $\text{sp}^3$  structures and different chemical-speciation AAEMs function together as the preferred active sites during steam gasification.  $\text{H}_2\text{O}/\text{HCl}$ -soluble AAEMs could promote the transformation of biochar surface functional groups, from ether/alkene C-O-C to carboxylate  $\text{COO}^-$  in biochar, while they may both be improved by  $\text{NH}_4\text{Ac}$ -soluble AAEMs.  $\text{H}_2\text{O}$ -soluble AAEMs play a crucial catalytic role in biochar reactivity. The effect of  $\text{NH}_4\text{Ac}$ -soluble AAEMs is mainly concentrated in the high-conversion stage (biochar conversion  $>30\%$ ), while that of  $\text{HCl}$ -soluble AAEMs is reflected in the whole activity-testing stage.

**Keywords:** biochar; steam; gasification; chemical speciation; AAEMs

## 1. Introduction

Compared to fossil fuels, biomass—which is a carbon neutral renewable energy, since the  $\text{CO}_2$  from its utilization can be captured via photosynthesis—exhibits great prospects for limiting global gas pollution ( $\text{NO}_x$ ,  $\text{SO}_2$  and greenhouse gases) and the energy crisis [1]. Biomass gasification is considered a promising technology with relatively lower temperatures, low energy consumption and a high ability of  $\text{CO}_2$  capture, attracting a lot of attention all over the world [2]. Usually, gasification can be divided into two steps, namely biomass devolatilization (first stage, relatively fast) and biochar gasification (second stage, relatively slow). According to previous studies [3–7], the gasification of pyrolysis biochar is the rate-limiting step for the overall gasification reaction, which is usually the focus of research on biomass gasification reactions. Besides, among the various gasifying agents (air, oxygen,  $\text{CO}_2$  and steam) for biomass/biochar gasification [8,9], steam is preferred for increasing the heating value of syngas and producing a gaseous fuel with relatively higher  $\text{H}_2$  for application in the fuel cells and hydrogen engines [10]. Thus, the steam gasification of pyrolysis biochar is urged to be investigated, especially for catalytic steam gasification [11], where the most important heterogeneous gasification reactions are the water gas reaction ( $\text{C} + \text{H}_2\text{O} \rightarrow \text{CO} + \text{H}_2$ ), the Boudouard reaction ( $\text{C} + \text{CO}_2 \rightarrow 2\text{CO}$ ) and the heterogeneous methanation ( $\text{C} + 2\text{H}_2 \leftrightarrow \text{CH}_4$ ) [12].

In the current investigation, many researchers [13–18] found that alkali and alkaline earth metallic species (AAEMs) dispersed in biomass and/or biochar as different chemical speciations, play significant catalytic roles in biochar gasification reactivity, and that AAEMs volatilized as a gaseous phase would also take part in homogeneous reforming reactions [19]. The concentration and dispersion of AAEMs, according to the results obtained by Wu et al. [20], is a significant factor affecting the catalytic activity of AAEMs during biomass gasification, which varies constantly due to the carbon consumption and the release/migration of AAEMs [21,22]. Moreover, for various gasifying agents, the AAEMs show different catalytic abilities when chars react with various gasifying agents such as H<sub>2</sub>O and CO<sub>2</sub>, because their catalysis mechanisms during biochar gasification may be different [19,23–25]. In addition, for the comparison of AAEM catalytic activities, Zhang et al. [26] studied the gasification reactivity of several biochar samples catalyzed by metals and reported that the gasification reactivity was enhanced with the alkali metals followed by alkaline earth metals. Furthermore, for the catalytic role of AAEMs on the microcosmic chemical bonds during gasification, the oxidation-reduction cycle [27–31] was postulated, in which O atoms/ions dissociated from the gasifying agents could be transferred to the carbon active sites through catalytically-active AAEMs, where the breakage of C-C bonds would occur to realize the liberation of the C(O) structure.

In addition, as our previous study mentioned [32], the AAEMs in biomass/biochar usually exist in a variety of chemical speciations, such as inorganic salts/ion states, organic forms linked to biochar and/or crystal forms. Jordan et al. [33] investigated the speciation and distribution of AAEMs in raw biomass and major ash-forming elements during gasification to evaluate the volatilization of these elements into the syngas, although they did not mention the state of AAEMs in biochar and their effects on the gasification reactivity of biochar. Besides, the catalytic effects of AAEMs with different chemical speciations on biochar reactivity are obviously different [34]. Thus, it is easy to deduce that their influence on the characteristics of biochar gasification would be significant, although relevant studies are rarely reported. In order to characterize the chemical speciation of AAEMs in biomass/biochar, a sequential selective extraction procedure known as chemical fractionation analysis (CFA) was introduced and standardized [35,36]. This method was first developed by Benson and Holm [37] for coals and had been modified by Zevenhoven-Onderwater et al. [38] and Petterson et al. [39] for biomass fuels. Moreover, besides their direct catalytic effects on biochar gasification, the AAEMs could have a dynamic impact on the biochar structures, including the carbon skeleton, side chains and functional groups [21,22,40]. It has been confirmed that the changes in biochar structure catalyzed by AAEMs are an important aspect influencing biochar reactivity during gasification [41]. However, there are few reports on the effect of AAEMs with different speciations on the biochar structure during gasification, which would in turn affect the biochar gasification reactivity. Biochar gasification can be significantly altered via the catalytic alteration of the above reaction pathways by different speciations of AAEMs. Thus a good understanding of the effect of the chemical speciation of AAEMs during biochar steam gasification would lay a solid foundation for developing a gasification technology for biomass.

The objectives are to understand the steam gasification behavior of pyrolysis biochar with different speciations of AAEMs, the key inherent chemical speciation of AAEMs affecting biochar reactivity, and the most probable catalytic route of AAEMs on biochar structure and reactivity during steam gasification, all of which are essential to gasification process design and development.

## 2. Experimental

### 2.1. Origin Biochar Preparation

Manchurian walnut sawdust, obtained from Harbin, Heilongjiang Province, China, was used in the experiments. The sawdust samples were dried overnight at 105 °C, pulverized and sieved to obtain a fraction with particle sizes between 0.15 and 0.25 mm. The proximate and ultimate analyses for the sawdust samples are listed in Table 1.

**Table 1.** Proximate and ultimate analysis of the origin sawdust sample. (Note: diff. = by difference, ad. = air dry basis.)

Samples	Proximate Analysis					Ultimate Analysis			
	M <sub>ad.</sub> (wt%)	A <sub>ad.</sub> (wt%)	V <sub>ad.</sub> (wt%)	FC <sub>ad.</sub> (wt%)	C <sub>ad.</sub> (wt%)	H <sub>ad.</sub> (wt%)	O <sub>ad.(diff.)</sub> (wt%)	N <sub>ad.</sub> (wt%)	S <sub>t,ad.</sub> (wt%)
Sawdust	9.49	0.96	77.13	12.42	43.72	5.31	40.39	0.12	0.01

As shown in Figure 1, the origin pyrolysis biochar samples were obtained in the entrained-flow reactor at 800 °C with nitrogen gas of 5.70 L/min. The details of the pyrolysis experimental system can be seen in our previous investigation [32]. The origin pyrolysis biochar was used for the following treatment and steam gasification.

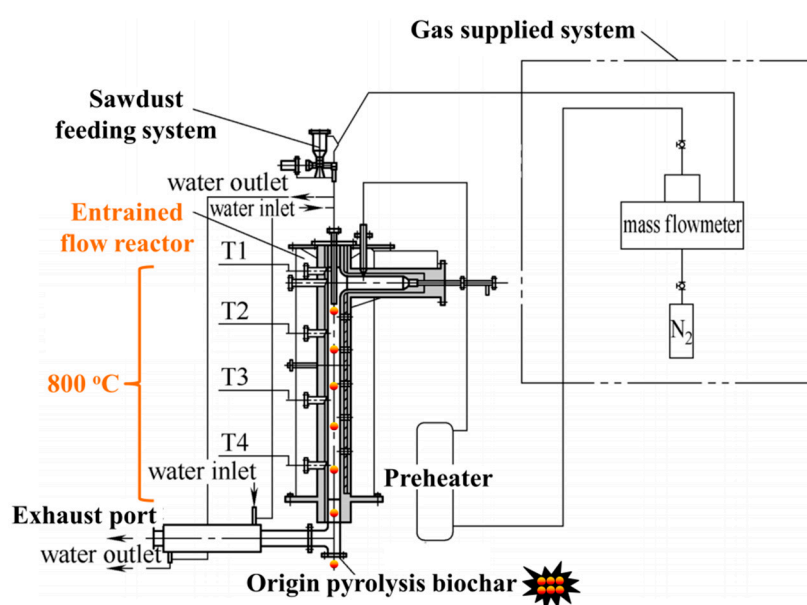


**Figure 1.** Schematic diagram of the entrained-flow reactor.

## 2.2. Sample Preparation

In order to investigate the effects of the solid-phase chemical speciation of AAEMs on the steam gasification of sawdust biochar, the CFA process was carried out. There are four kinds of chemical speciation of AAEMs in biochar [42]: One is a separate form of AAEM ions, which is soluble in water, also soluble in a solution of ammonium acetate (NH<sub>4</sub>Ac) and hydrochloric acid (HCl); The second is organic matter, which is in the form of carboxylate and/or coordination connected with the oxygen functional groups on the biochar surface, and is insoluble in water, but soluble in a solution of NH<sub>4</sub>Ac and HCl; The third is attached to the clay surface in an amorphous form, which is insoluble in water and NH<sub>4</sub>Ac solution, but soluble in hydrochloric acid; The fourth is in the aluminosilicate form, which is insoluble in water, NH<sub>4</sub>Ac and HCl. In the CFA process, as shown in Figure 2, the pyrolysis biochar is leached step-wise in increasingly aggressive solvents: deionized water, 1.0 mol/L ammonium acetate solution, and 1.0 mol/L hydrochloric acid solution with a mass ratio (1:30) of solid to liquid, in order to classify the AAEMs with respect to solubility.

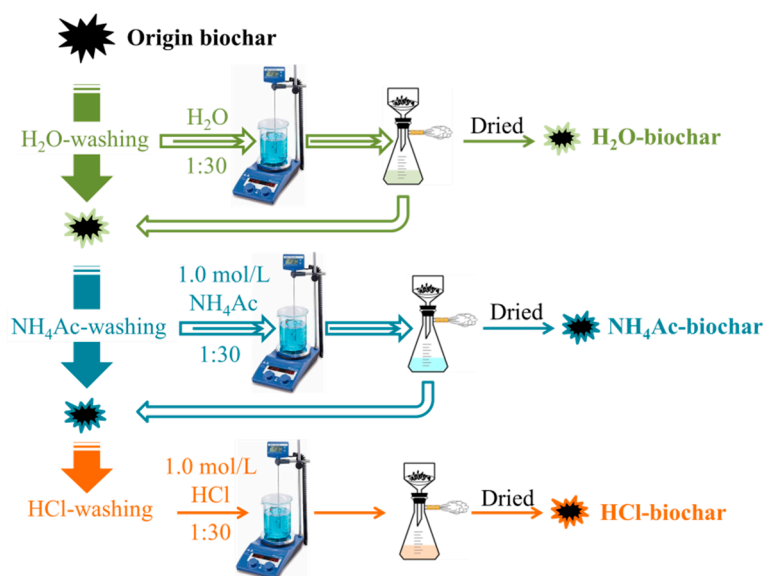


Figure 2. Schematic of the chemical fractionation analysis of biochar.

### 2.3. Steam Gasification of Biochar

As shown in Figure 3, the steam gasification of sawdust biochar was carried out. A total of 0.5 g of biochar from the CFA, namely the origin-biochar/H<sub>2</sub>O-biochar/NH<sub>4</sub>Ac-biochar/HCl-biochar samples, were pre-loaded into the top fixed-bed stage of the reactor. After being purged for 5 min by argon (Ar), the system was heated up to 800 °C with argon gas of 1.53 L/min at a heating rate of 20 °C/min. As the temperature stabilized at 800 °C, the atmosphere was switched to 15 vol% steam for the gasification reaction, which was achieved by feeding deionized water of 0.214 L/min through a high-performance liquid chromatography (HPLC) pump into the heated zone of reactor where the water was evaporated into steam directly. The steam gasification reaction of biochar at 800 °C lasted for 10 min. After that, reactions were terminated by switching the atmosphere to argon and removing the reactor from the furnace. Argon was passed through the reactor until the reactor had completely cooled to room temperature to avoid oxidation. The steam gasification biochar was collected and stored at 4 °C for further analysis.

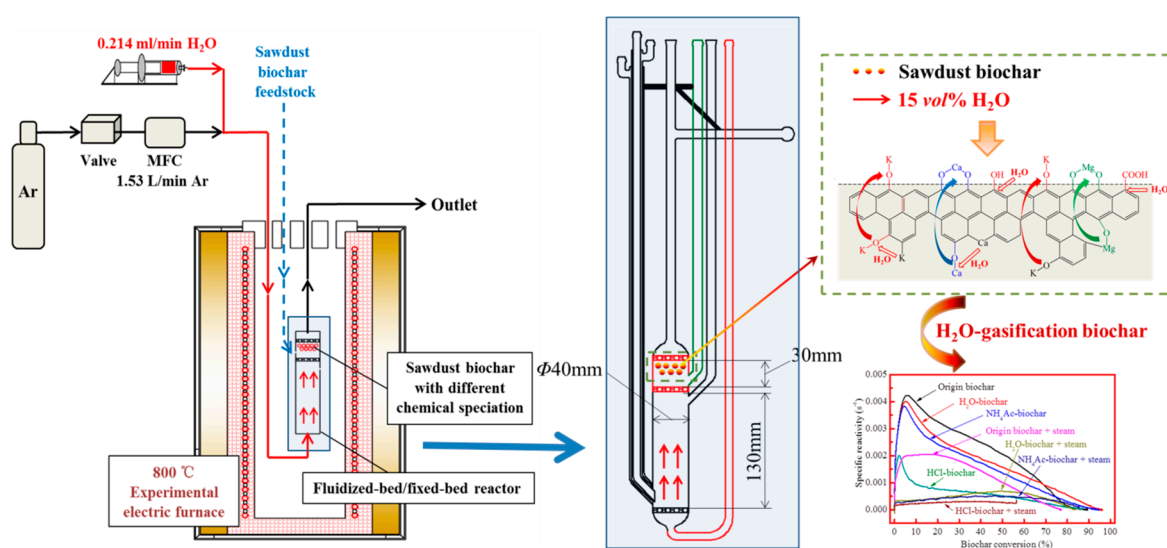


Figure 3. A schematic diagram of the steam gasification experimental process.

## 2.4. Analysis of Biochar

### 2.4.1. Gasification Rate

The gasification rate of biochar was measured three times by weighing the biochar-containing reactor before and after the reactions. Each experiment was repeated at least three times, and the test results are well-reproducible.

### 2.4.2. AAEM Analysis

The chemical speciation of AAEMs in biochar was quantified by inductively-coupled plasma-atomic emission spectroscopy (ICP-AES). The biochar sample (0.1 g) was digested in a 1:3:8 (*v/v/v*) mixture of 40% HF, 30% H<sub>2</sub>O<sub>2</sub>, and 65% HNO<sub>3</sub> at 200 °C for 60 min.

The percentage of AAEMs released during the steam gasification of biochar can be obtained by Equation (1) as follows:

$$X_{\text{Release}} \% = \left[ 1 - X_{\text{Steam gasification biochar}} \times \frac{(1 - \text{Gasification rate})}{X_{\text{Pyrolysis biochar}}} \right] \times 100\% \quad (1)$$

where *X* is the AAEM species (Na, K, Mg and Ca); *X*<sub>Release</sub> is the percentage of AAEM release during the steam gasification of biochar; *X*<sub>Pyrolysis biochar</sub> is the *X* in origin/H<sub>2</sub>O-/NH<sub>4</sub>Ac-/HCl-pyrolysis biochar; and *X*<sub>Steam gasification biochar</sub> is the *X* in origin/H<sub>2</sub>O-/NH<sub>4</sub>Ac-/HCl-steam gasification biochar.

### 2.4.3. Raman Analysis

The aromatic structure analysis of biochar was carried out in a Raman spectrometer (inVia, Renishaw, New Mills, UK), with an excitation laser at 633 nm. The sample was mixed and ground with spectroscopic-grade Potassium bromide (KBr) in the ratio of 0.25 wt% biochar. The Raman spectra at 800~1800 cm<sup>-1</sup> were recorded.

### 2.4.4. FTIR Analysis

The surface functional groups of the biochar were analyzed by Fourier Transform infrared spectroscopy (Nicolet 5700, FTIR, Thermo Fisher Scientific, Waltham, MA, USA). Biochar was mixed and ground with spectroscopic-grade KBr in a ratio of 1:200. All FTIR spectra were obtained at a resolution of 4 cm<sup>-1</sup> in the range of 400~4000 cm<sup>-1</sup>.

### 2.4.5. Biochar Reactivity Analysis

The specific reactivity of the biochar was determined in air at 370 °C with a thermogravimetric analyzer (TGA: Mettler Toledo, Switzerland). Nearly 4 mg of biochar sample was placed in a Pt crucible and heated in Ar in the TGA to 105 °C to remove moisture from the sample. The stabilized weight of the biochar at 105 °C was taken as the weight of dry biochar. The temperature was then increased to 370 °C at 50 °C/min. After 2 min, the atmosphere was switched into air starting the biochar reactivity test. Once the mass was stable, the sample was heated at 50 °C/min to 600 °C, where it was held for another 30 min to ensure complete combustion. The calculation of biochar-specific reactivity from the differential thermal gravity (DTG) data (dW/dt) can be seen in our previous study [22].

## 3. Results and Discussion

### 3.1. Steam Gasification Rate

As shown in Figure 4, it can be seen that the steam gasification rate of pyrolysis biochar after the fraction of H<sub>2</sub>O, NH<sub>4</sub>Ac and HCl decreased sequentially, from 79.00% of origin biochar to 66.54% of HCl-biochar. Our previous investigation [43] indicated that during the chemical fractionation analysis, the changes in oxygen-containing functional groups and aromatic ring structures could be ignored.

It can be speculated that the difference in the gasification rate is mainly caused by the different chemical speciation of the AAEM species. The difference in gasification rate was used to describe the effect of different-speciation AAEMs on the steam gasification reaction of biochar, as shown in Figure 4. The decrease of 5.81% in the steam gasification rate from origin biochar to H<sub>2</sub>O-biochar sample is entirely due to the removal of H<sub>2</sub>O-soluble AAEMs, and this part mainly deals with K<sup>+</sup> and Na<sup>+</sup> ion salts in biochar [32]. After that, the decline of the biochar steam gasification rate is gradually reduced, to 4.20% and 2.45% due to the removal of the NH<sub>4</sub>Ac-soluble and HCl-soluble AAEMs, respectively. Finally, the HCl-biochar sample, with only some insoluble aluminosilicate AAEMs, still retains a relative high gasification rate (as 66.54%), mainly due to the relatively active carbon structures and the insoluble AAEMs to maintain the basic reactions between carbon and steam.

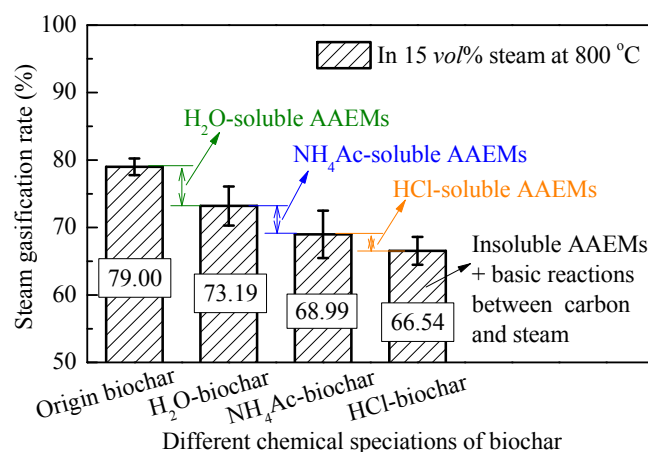


Figure 4. Steam gasification rate of biochar from chemical analysis fractionation.

### 3.2. AAEM Analysis of Steam-Gasified Biochar

Figure 5 shows the AAEM content of the origin pyrolysis biochar and their chemical speciation. In the original pyrolysis biochar at 800 °C, the AAEMs exhibited a rich distribution of K (0.70 wt%) and Ca (2.08 wt%), and less Na (0.05 wt%) and Mg (0.17%). Besides, the main existing form of K in pyrolysis biochar is a water-soluble form, while that of Ca is a NH<sub>4</sub>Ac-soluble and insoluble form. As Mitsuoka et al. [44] suggested, the most significant catalysts for biochar gasification in woody biomass are calcium (Ca) and potassium (K), namely the two main kinds of AAEM.

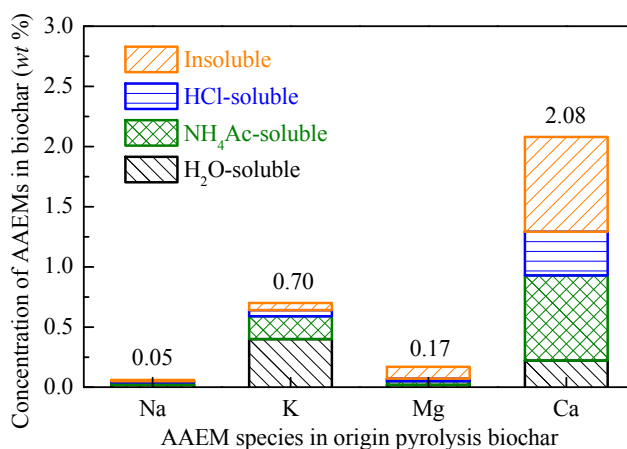


Figure 5. Concentration of AAEMs in origin pyrolysis biochar.

As mentioned above, the role of AAEMs is not only in the solid-phase heterogeneous transformation of biochar, their migration and precipitation characteristics also play a significant role in homogeneous steam reform. It is often agreed that the volatilization of AAEMs occurs during gasification [45,46]. According to Marschner et al. [47], the behavior of Na and K were different from that of Mg and Ca, at least partly due to the different chemical status of K/Na and Mg/Ca in the biomass/biochar. It is also related to the different occurrence of K/Na and Mg/Ca. For the H<sub>2</sub>O-soluble AAEMs, the specific precipitation amount of AAEMs cannot be calculated directly by the difference in this paper. However, the total amount of AAEMs in the fractional speciation can be calculated to characterize the precipitation of AAEMs in the absence of H<sub>2</sub>O-soluble ones. This effectively avoids the influence of AAEM transformation with different chemical speciations during steam gasification [33].

The release of K and Ca during the steam gasification of biochar can be seen in Figure 6.  $K_{\text{Release}}$  and  $Ca_{\text{Release}}$  did not change significantly after H<sub>2</sub>O washing, and it can be seen that the H<sub>2</sub>O-washing removal amount and the amount of volatilization during the gasification of K and Ca were very close, indicating that the precipitation rate of H<sub>2</sub>O-soluble K and Ca was close to 100%. After the fraction of NH<sub>4</sub>Ac and HCl solution, the  $K_{\text{Release}}$  was significantly reduced and  $Ca_{\text{Release}}$  was still relatively high, indicating that during gasification the release of K occurs mainly in the form of inorganic salts and hydrated ions, while volatilization of the organic compounds is the main release mechanism for Ca.

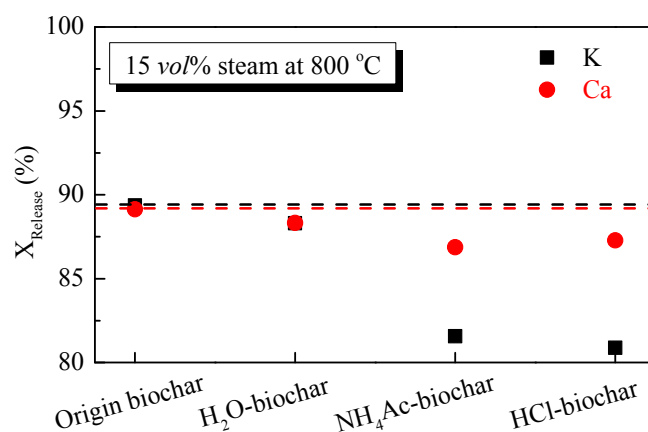


Figure 6. Release of K and Ca species during the steam gasification of biochar.

### 3.3. Raman Analysis of Steam-Gasified Biochar

As shown in Figure 7, the total Raman area between 800 and 1800 cm<sup>-1</sup> of the pyrolysis biochar samples from the CFA process changed little, with a total intensity of 1.62~1.72 × 10<sup>6</sup>. The total Raman peak areas could reflect electron-rich structures such as O/N-containing functional groups in biochar [48–51]. During the steam gasification of biochar, it can be seen that the total Raman areas of gasified biochar decreased from 3.58 × 10<sup>6</sup> to 2.23 × 10<sup>6</sup> with the fractionation of H<sub>2</sub>O, NH<sub>4</sub>Ac and HCl in turn. According to Guo et al. [41], both the thermal decomposition of biochar, and biochar gasification reactions leading to the loss of oxygen and hydrogen from biochar, could result in changes to biochar structures during gasification with a decrease of total Raman intensity. Also, another possible factor may be the preferential consumption of smaller rings due to their gasification and/or conversion to larger ones. Briefly, during steam gasification, the decrease in Raman intensity with the CFA process reflected the limited increase in O-containing functional groups and, more importantly, the condensation/growth of aromatic ring systems. For the HCl-biochar, with few active AAEMs (in the absence of catalysts), the O-containing functional groups formed in the biochar during steam gasification were closely associated with the aromatic structure and thus tended to loosen the aromatic structure. The non-catalyzed gasification was slow and took place on some specific (especially sp<sup>3</sup>-rich or sp<sup>2</sup>-sp<sup>3</sup> mixture) sites distributed throughout the biochar [52]. While the gasification of biochar

took place everywhere but slowly in the HCl-biochar in order to consume the small ring systems selectively, the reaction in the AAEM-containing biochar was more focused on/around the AAEM sites and took place much more rapidly [53]. As shown in Figure 7, comparing the results of steam-gasified origin biochar and H<sub>2</sub>O-biochar samples, there is a significant decrease of  $0.65 \times 10^6$ , showing that the increase of surface O-containing functional groups during gasification was limited after the fraction of H<sub>2</sub>O, mainly due to the H<sub>2</sub>O-soluble AAEMs, namely the K and Na species. For the total Raman area between gasified H<sub>2</sub>O-biochar and NH<sub>4</sub>Ac-biochar, the decrease was only  $0.22 \times 10^6$ , showing that the effects of NH<sub>4</sub>Ac-soluble AAEMs were limited. Although the AAEM content is relatively large, their low ability of migration led to a limited catalytic role. After that, the effect of HCl-soluble AAEMs, namely the organic Ca species, led to another obvious decrease of  $0.48 \times 10^6$  in the total Raman area, showing its significant catalytic role on the formation of surface O-containing functional groups.

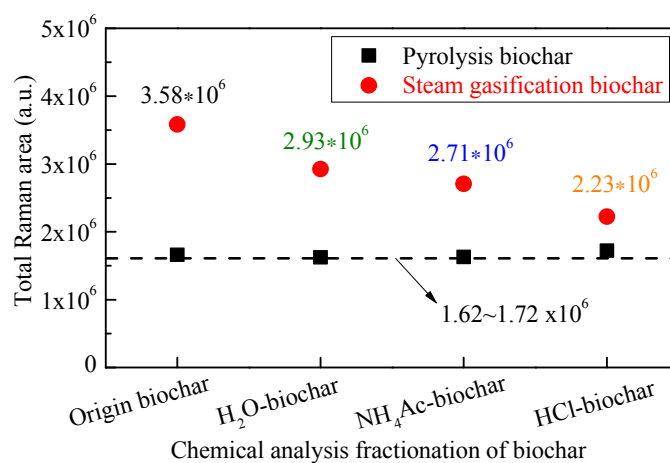


Figure 7. Total Raman area of biochar during steam gasification.

As shown in Figure 8, the Raman spectrum of the gasified biochar was divided into 10 small peaks, representing the typical structures of biochar. Other detailed information on this part can be seen in our previous studies [19,32], where the  $I_{(D_r+V_l+V_r)}/I_D$  represents the ratio of the smaller aromatic rings in the biochar to the larger aromatic ring structures, and  $I_S/I_{Total}$  refers to the content of sp<sup>3</sup>-rich structures as alkyl-aryl C-C structures and methyl carbon dangling to an aromatic ring, including some surface O-containing structures in biochar, with little long chain aliphatics and hydroaromatic structures.

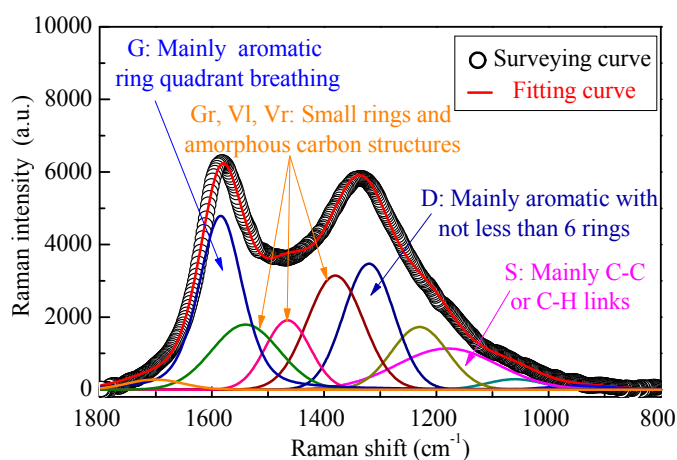


Figure 8. Curve fitting of the Raman spectrum of biochar.

As shown in Table 2, the influence of chemical fraction analysis on biochar aromatic ring structures could be ignored, while both  $\text{NH}_4\text{Ac}$  and  $\text{HCl}$  can change the cross-linking structures of biochar [43]. During steam gasification, according to Chen et al. [54], the sites on either the zigzag face or the armchair face of large aromatic layers of biochar are believed to be active for gasification reactions and they are affected by AAEMs. In addition, according to Li et al. [52], the smaller aromatic ring systems were preferentially consumed during gasification. During the steam gasification of biochar, with the presence of  $\text{H}_2\text{O}$ -soluble AAEMs, the  $I_{(\text{Dr}+\text{Vl}+\text{Vr})}/I_{\text{D}}$  decreased significantly from 1.84 to 0.64, indicating the transformation of the smaller aromatic ring systems into larger ones to a great extent. The conversion of biochar during steam gasification is believed to be due to the rapid penetration of H radicals from the biochar surface deep into the biochar matrix [55]. Also the AAEMs, as the active sites for the gasification reaction, could promote the process of this transformation to a large extent, especially for the alkali metal species (K and Na). With the fraction of  $\text{NH}_4\text{Ac}$  and  $\text{HCl}$  solutions, the decrease of  $I_{(\text{Dr}+\text{Vl}+\text{Vr})}/I_{\text{D}}$  became more and more weak, showing the smaller catalytic effect of  $\text{NH}_4\text{Ac}/\text{HCl}$ -soluble AAEMs on the aromatic ring structures in biochar. As shown in Table 2, due to the steam gasification of  $\text{HCl}$ -biochar, the  $I_{\text{S}}/I_{\text{Total}}$  decreased from 0.18 to 0.10. These data indicate that the  $\text{sp}^3$ -rich or  $\text{sp}^2$ - $\text{sp}^3$  mixed structures represented by the S band are the preferential sites of reaction with steam with few active AAEMs catalysts, with only insoluble ones left. The results are consistent with the opinion of Li et al. [52] for coal char. In addition, the effect of the  $\text{NH}_4\text{Ac}/\text{HCl}$ -soluble AAEMs is limited as the active site during gasification, and consequently the corresponding  $I_{\text{S}}/I_{\text{Total}}$  decreases, since the  $\text{sp}^3$ -rich or  $\text{sp}^2$ - $\text{sp}^3$  structures are consumed. However, few changes in the relative intensity of S band were observed for the corresponding biochars from the origin biochar during gasification (from 0.38 to 0.37). This indicated that with the  $\text{H}_2\text{O}$ -soluble AAEMs, the S band structures were no longer the preferred sites for reactions with steam. The AAEM catalytic species appeared to be preferentially accommodated on carbons of an aromatic nature.

**Table 2.** Ratios of band peak areas in pyrolysis and steam gasification biochar from Chemical fractionation analysis (CFA).

Conditions	Band Ratio	Origin Biochar	$\text{H}_2\text{O}$ -Biochar	$\text{NH}_4\text{Ac}$ -Biochar	$\text{HCl}$ -Biochar
Pyrolysis	$I_{(\text{Vl}+\text{Dr}+\text{Vr})}/I_{\text{D}}$	1.84	1.97	2.06	2.19
	$I_{\text{S}}/I_{\text{Total}}$	0.38	0.34	0.22	0.18
Gasification	$I_{(\text{Vl}+\text{Dr}+\text{Vr})}/I_{\text{D}}$	0.64	1.51	1.91	2.02
	$I_{\text{S}}/I_{\text{Total}}$	0.37	0.28	0.17	0.10

### 3.4. FTIR Analysis of Steam-Gasified Biochar

The CFA process has less destructive effects on the surface carbon–oxygen functional groups of pyrolysis biochar, which was already present in our previous study [43]. With the result of the total Raman area related with the surface functional groups, the additional O-containing functional groups were not present in the pyrolysis biochar before steam gasification. To gain evidence for the formation of additional O-containing functional groups during gasification, the FTIR spectra of the biochar samples were recorded, as shown in Figure 9. According to Černý et al. [56], the FTIR spectra of  $4000\sim 400\text{ cm}^{-1}$  are divided into  $3600\sim 3000\text{ cm}^{-1}$ ,  $3000\sim 2800\text{ cm}^{-1}$ ,  $1800\sim 1000\text{ cm}^{-1}$  and  $900\sim 700\text{ cm}^{-1}$ , which represent the surface hydroxyl group, aliphatic hydrocarbons, oxygen-containing functional groups, and aromatic hydrocarbons, respectively. As shown in Figure 9, for the steam-gasified biochar with different chemical fractions, the main difference appears in the oxygen-containing functional groups. In order to describe in detail the changes in the various oxygen-containing functional groups, the FTIR curve was fitted into the aromatic  $\text{C}=\text{C}$  structure at  $1480\text{ cm}^{-1}$ , the carboxylate  $\text{COO}^-$  structure at  $1400\text{ cm}^{-1}$  and the aromatic ether/alkene  $\text{C}-\text{O}-\text{C}$  at  $1243$  and  $1080\text{ cm}^{-1}$  [57,58].

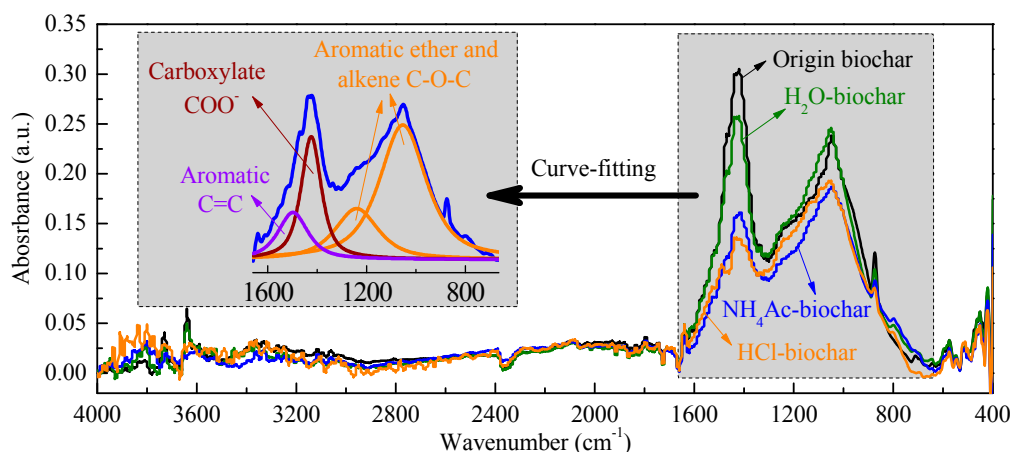


**Figure 9.** FTIR analysis of steam-gasified biochar with different chemical fractions.

The result of the curve-fitting FTIR analysis on O-containing functional groups can be seen in Table 3.

**Table 3.** FTIR analysis of O-containing functional groups on steam-gasified biochar surface.

Steam-Gasified Biochar	Surface Main Functional Groups		
	Aromatic C=C	Carboxylate COO <sup>−</sup>	Aromatic Ether/Alkene C-O-C
Gasified origin biochar	10.63	26.46	62.90
Gasified H <sub>2</sub> O-biochar	9.94	21.82	68.23
Gasified NH <sub>4</sub> Ac-biochar	10.27	14.10	75.62
Gasified HCl-biochar	11.39	9.98	78.62

The FTIR curve between the two successive steps can be used to indirectly reflect the specific catalytic effect of different AAEMs on the formation of oxygen-containing functional groups during steam gasification. Walker and co-workers [59] have also pointed out in a review that a significant amount of O complex builds up on the surface of active sites, which is referred to the AAEMs. The content of aromatic C=C on the steam gasified biochar from different CFA processes fluctuated in the range of 9.94~11.39%, with little change. In addition, the main changes existed between the carboxylate COO<sup>−</sup> and aromatic ether/alkene C-O-C. In the absence of active AAEMs, the HCl-biochar exhibits the lowest surface functional group content, which is consistent with the Raman analysis results. The HCl-soluble AAEMs (mainly for the organic Ca compounds mentioned above), are mainly used to promote the formation of carboxylate COO<sup>−</sup> (from 9.98% to 14.10%), and to limit the increase of aromatic ether/alkene C-O-C (from 78.62% to 75.62%), which can be considered to be the transformation from ether/alkene C-O-C to carboxylate COO<sup>−</sup> catalyzed by HCl-soluble AAEMs. However, for the NH<sub>4</sub>Ac-soluble AAEMs, as shown in Figure 9, the relative contents of carboxylate COO<sup>−</sup> and aromatic ether/alkene C-O-C were both significantly improved, indicating that the AAEMs played a positive role in promoting the formation of surface oxygen-containing functional groups. Compared to the FTIR results for the origin biochar and the H<sub>2</sub>O-biochar after gasification, the catalytic effect of the H<sub>2</sub>O-soluble AAEMs in biochar was investigated. A similar result can be seen in that during the steam gasification, the H<sub>2</sub>O-soluble AAEMs promote the increase of the total amount of oxygen-containing functional groups, and the catalytic effect on the increase of carboxylate COO<sup>−</sup> is the most significant.

### 3.5. Biochar Reactivity in Air

The specific reactivity of biochar in combustion as a function of biochar conversion can be seen in Figure 10. As usual, the biochar reactivity is mainly controlled by two factors: the biochar structure [60]

and AAEM species in biochar [3]. The chemical fractionation process has little effect on the pyrolysis biochar structure [43], thus the AAEMs in the biochar are considered to be the main controlling factor affecting the pyrolysis biochar activity in this experiment. Given the high quantities of AAEMs and their possible catalytic activities, the catalytic activity of AAEMs may be the most likely factor causing the difference in reactivity, because reactions under a steam atmosphere make a difference in the concentration and dispersion of AAEMs in the resulting chars [40]. During steam gasification, the AAEMs only increase the concentration of the active complexes on carbon rather than changing the reaction pathway [61–65]. Figure 10 shows the typical specific reactivity of the pyrolysis biochar samples from the CFA process. After the chemical fractionation, the content of AAEMs decreased gradually, resulting in a decrease of the total reaction activity of the pyrolysis biochar. The specific reactivity showed broad maxima at about 5.8%, 5.2%, 5.0% and 2.0% char conversions for the pyrolysis origin biochar, H<sub>2</sub>O-biochar, NH<sub>4</sub>Ac-biochar and HCl-biochar, respectively. The maximum reactivity tended to shift towards lower conversion levels with the CFA steps. The main reason for the initial increase in the biochar reactivity (Figure 10) at small biochar conversion levels was the accumulation of AAEMs on the biochar surface with the removal of carbonaceous matter. During the air gasification of biochar, the high mobility of AAEMs allows them to migrate onto the biochar surface to form catalytically-active species such as –O-AAEM and/or AAEM clusters [66]. At high biochar conversion levels, where the biochar structure is more inert and highly condensed, the catalytic activity of AAEMs is reduced compared to its activity at low biochar conversion levels. In other words, at the beginning, the increase of AAEMs on the biochar surface are the main factor influencing the biochar reactivity. At a later stage, changes in the biochar structure become significant. The preferential removal of smaller aromatic ring systems and the persistence of crosslinking structures mean that the large aromatic ring systems are increasingly concentrated with little flexibility [52].

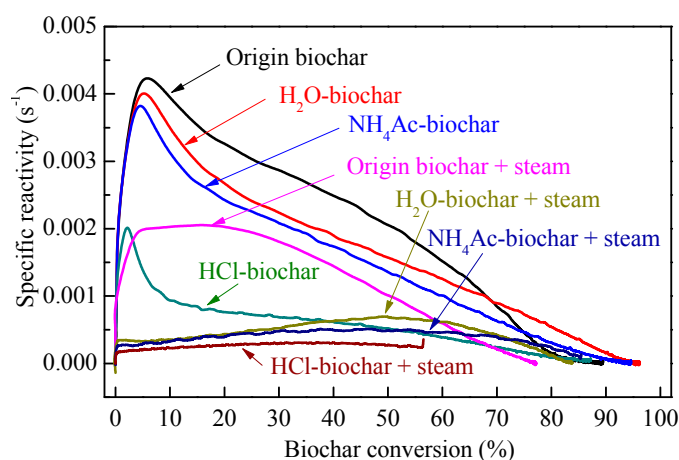


**Figure 10.** Specific reactivity of biochar samples as a function of biochar conversion.

For the steam-gasified biochar samples, the catalytic activity of AAEMs is a result of the interaction between AAEMs and biochar/carbon structures. As in the initial stage of the biochar reactivity test, unlike the pyrolytic one, there were significant differences in the biochar structure (i.e., O-containing functional groups and aromatic structures) by CFA in the steam gasification process. Furthermore, the AAEM-containing species in the biochar during the steam gasification improved the O-containing functional groups that would be consumed quickly during the reactivity measurement, contributing to the increase in reactivity [67], while the AAEMs would decrease the relative content of small aromatic ring structures in the biochar during steam gasification leading to the decrease in reactivity. Thus, the final decision of the steam-gasified biochar depends on the synergetic effects of the biochar structure and AAEMs [22]. According to Li et al. [68], the AAEMs would not be volatilized during the oxidation of biochar with air in the TGA at 370 °C during the measurement of biochar reactivity. However, during

gasification, it can be seen from Section 3.4 that the AAEMs could be significantly precipitated, especially for the H<sub>2</sub>O-soluble AAEMs (nearly 100% volatilization). As shown in Figure 10, there is a significant decrease of biochar reactivity between the “origin biochar + steam” and the other three samples. For the biochar gasification in 15 vol% steam at 800 °C, the water-soluble AAEMs play a crucial role in the catalytic activity of gasification biochar. Despite its nearly complete volatilization, the water-soluble AAEMs have a significant effect on the biochar structure, which is a key factor in determining the highest reactivity of the biochar. The difference between “H<sub>2</sub>O-biochar + steam” and “NH<sub>4</sub>Ac-biochar + steam” is mainly concentrated in the higher carbon conversion stage (biochar conversion >30%), which is mainly due to the biochar structure determining the reaction [66]. The effect of HCl-soluble AAEMs on the biochar reactivity functions from start to finish. For “HCl-biochar + steam”, the reactivity is the lowest, mainly due to the least amount of catalytically active elements (AAEMs) and the less active structure formation in the biochar.

#### 4. Conclusions

- (1) The AAEMs in different chemical speciations, such as the H<sub>2</sub>O/NH<sub>4</sub>Ac/HCl-soluble ones, have significant effects on the steam gasification rate of sawdust biochar. During steam gasification, the release of K occurs mainly in the form of inorganic salts and hydrated ions, while the release of Ca is mainly for the organic ones.
- (2) During steam gasification, the limited increase of O-containing functional groups and, more importantly, the condensation/growth of aromatic ring systems existed for the AAEMs with different chemical speciations. Without the active AAEMs (such as HCl-biochar), the sp<sup>3</sup>-rich or sp<sup>2</sup>-sp<sup>3</sup> structures are the preferred sites for steam gasification. With NH<sub>4</sub>Ac/HCl-soluble AAEMs, the preferred sites with sp<sup>3</sup>-rich or sp<sup>2</sup>-sp<sup>3</sup> structures are gradually shared by AAEMs, until the presence of H<sub>2</sub>O-soluble AAEMs completely replaces them as the gasification sites.
- (3) H<sub>2</sub>O/HCl-soluble AAEMs promote the transformation from ether/alkene C-O-C to carboxylate COO<sup>-</sup> while promoting the increase of total surface oxygen functional groups. The relative contents of carboxylate COO<sup>-</sup> and aromatic ether/alkene C-O-C were significantly improved by the NH<sub>4</sub>Ac-soluble AAEMs.
- (4) The H<sub>2</sub>O-soluble AAEMs play a crucial role in the catalytic activity of gasification biochar and is a key factor in determining its highest reactivity. The effect of NH<sub>4</sub>Ac-soluble AAEMs on gasification biochar activity is mainly concentrated in the high carbon conversion stage (biochar conversion >30%), and the effect of HCl-soluble AAEMs is reflected in the whole activity-testing stage.

**Acknowledgments:** The Collaborative Innovation Center of Clean Coal Power Plant with Poly-Generation, the national key R&D program of China (2016YFE0102500) and the National Natural Science Foundation innovation research group Heat Transfer and Flow Control (51421063) are gratefully acknowledged.

**Author Contributions:** D.F., Y.Z. and S.S. conceived and designed the experiments; D.F. and Y.Z. performed the experiments; D.F., J.G. and Y.Z. analyzed the data; J.G. and Y.Z. contributed reagents/materials/analysis tools; D.F. wrote the paper.

**Conflicts of Interest:** The authors declare no conflict of interest.

#### Nomenclature

AAEMs	Alkali and alkaline earth metallic species
X	AAEMs (Na, K, Mg and Ca)
X <sub>Release</sub>	X(AAEMs) release during gasification
X <sub>Pyrolysis biochar</sub>	X(AAEMs) in pyrolysis biochar
X <sub>Steam gasification biochar</sub>	X(AAEMs) in steam gasification biochar
CFA	Chemical fractionation analysis
NH <sub>4</sub> Ac	Ammonium acetate
H <sub>2</sub> O-soluble	Soluble in water
NH <sub>4</sub> Ac-soluble	Soluble in NH <sub>4</sub> Ac solution

HCl-soluble	Soluble in HCl solution
Insoluble	Insoluble in water/NH <sub>4</sub> Ac/HCl
H <sub>2</sub> O	Deionized water
HCl	Hydrochloric acid
Origin-biochar	Origin pyrolysis biochar
H <sub>2</sub> O-biochar	H <sub>2</sub> O-washed biochar
NH <sub>4</sub> Ac-biochar	NH <sub>4</sub> Ac-washed biochar
HCl-biochar	HCl-washed biochar

## References

1. Damartzis, T.; Zabaniotou, A. Thermochemical conversion of biomass to second generation biofuels through integrated process design—A review. *Renew. Sustain. Energy Rev.* **2011**, *15*, 366–378. [[CrossRef](#)]
2. Parthasarathy, P.; Narayanan, K.S. Hydrogen production from steam gasification of biomass: Influence of process parameters on hydrogen yield—A review. *Renew. Energy* **2014**, *66*, 570–579. [[CrossRef](#)]
3. Li, C.-Z. Importance of volatile–char interactions during the pyrolysis and gasification of low-rank fuels—A review. *Fuel* **2013**, *112*, 609–623. [[CrossRef](#)]
4. Nowicki, L.; Markowski, M. Gasification of pyrolysis chars from sewage sludge. *Fuel* **2015**, *143*, 476–483. [[CrossRef](#)]
5. Qi, X.; Guo, X.; Xue, L.; Zheng, C. Effect of iron on Shenfu coal char structure and its influence on gasification reactivity. *J. Anal. Appl. Pyrolysis* **2014**, *110*, 401–407. [[CrossRef](#)]
6. Duman, G.; Uddin, M.A.; Yanik, J. The effect of char properties on gasification reactivity. *Fuel Proc. Technol.* **2014**, *118*, 75–81. [[CrossRef](#)]
7. Liu, L.; Cao, Y.; Liu, Q. Kinetics studies and structure characteristics of coal char under pressurized CO<sub>2</sub> gasification conditions. *Fuel* **2015**, *146*, 103–110. [[CrossRef](#)]
8. Shen, Y.; Zhao, P.; Shao, Q.; Ma, D.; Takahashi, F.; Yoshikawa, K. In-situ catalytic conversion of tar using rice husk char-supported nickel-iron catalysts for biomass pyrolysis/gasification. *Appl. Catal. B Environ.* **2014**, *152–153*, 140–151. [[CrossRef](#)]
9. Kirtania, K.; Joshua, J.; Kassim, M.A.; Bhattacharya, S. Comparison of CO<sub>2</sub> and steam gasification reactivity of algal and woody biomass chars. *Fuel Proc. Technol.* **2014**, *117*, 44–52. [[CrossRef](#)]
10. Luo, S.; Xiao, B.; Hu, Z.; Liu, S.; Guo, X.; He, M. Hydrogen-rich gas from catalytic steam gasification of biomass in a fixed bed reactor: Influence of temperature and steam on gasification performance. *Int. J. Hydrogen Energy* **2009**, *34*, 2191–2194. [[CrossRef](#)]
11. Li, C.-Z. Special issue—Gasification: A route to clean energy. *Proc. Saf. Environ. Prot.* **2006**, *84*, 407–408. [[CrossRef](#)]
12. Nanou, P.; Gutiérrez Murillo, H.E.; van Swaaij, W.P.M.; van Rossum, G.; Kersten, S.R.A. Intrinsic reactivity of biomass-derived char under steam gasification conditions-potential of wood ash as catalyst. *Chem. Eng. J.* **2013**, *217*, 289–299. [[CrossRef](#)]
13. Kajita, M.; Kimura, T.; Norinaga, K.; Li, C.-Z.; Hayashi, J.-I. Catalytic and noncatalytic mechanisms in steam gasification of char from the pyrolysis of biomass. *Energy Fuels* **2009**, *24*, 108–116. [[CrossRef](#)]
14. Eom, I.-Y.; Kim, J.-Y.; Kim, T.-S.; Lee, S.-M.; Choi, D.; Choi, I.-G.; Choi, J.W. Effect of essential inorganic metals on primary thermal degradation of lignocellulosic biomass. *Bioresour. Technol.* **2012**, *104*, 687–694. [[CrossRef](#)] [[PubMed](#)]
15. Lahijani, P.; Zainal, Z.A.; Mohamed, A.R.; Mohammadi, M. CO<sub>2</sub> gasification reactivity of biomass char: Catalytic influence of alkali, alkaline earth and transition metal salts. *Bioresour. Technol.* **2013**, *144*, 288–295. [[CrossRef](#)] [[PubMed](#)]
16. Yu, M.M.; Masnadi, M.S.; Grace, J.R.; Bi, X.T.; Lim, C.J.; Li, Y. Co-gasification of biosolids with biomass: Thermogravimetric analysis and pilot scale study in a bubbling fluidized bed reactor. *Bioresour. Technol.* **2015**, *175*, 51–58. [[CrossRef](#)] [[PubMed](#)]
17. Zolin, A.; Jensen, A.; Jensen, P.A.; Frandsen, F.; Dam-Johansen, K. The influence of inorganic materials on the thermal deactivation of fuel chars. *Energy Fuels* **2001**, *15*, 1110–1122. [[CrossRef](#)]

18. Long, J.; Song, H.; Jun, X.; Sheng, S.; Lun-shi, S.; Kai, X.; Yao, Y. Release characteristics of alkali and alkaline earth metallic species during biomass pyrolysis and steam gasification process. *Bioresour. Technol.* **2012**, *116*, 278–284. [[CrossRef](#)] [[PubMed](#)]
19. Feng, D.; Zhao, Y.; Zhang, Y.; Sun, S. Effects of H<sub>2</sub>O and CO<sub>2</sub> on the homogeneous conversion and heterogeneous reforming of biomass tar over biochar. *Int. J. Hydrogen Energy* **2017**, *42*, 13070–13084. [[CrossRef](#)]
20. Wu, H.; Quyn, D.M.; Li, C.-Z. Volatilisation and catalytic effects of alkali and alkaline earth metallic species during the pyrolysis and gasification of Victorian brown coal. Part III. The importance of the interactions between volatiles and char at high temperature. *Fuel* **2002**, *81*, 1033–1039. [[CrossRef](#)]
21. Feng, D.; Zhao, Y.; Zhang, Y.; Zhang, Z.; Sun, S. Roles and fates of K and Ca species on biochar structure during in-situ tar H<sub>2</sub>O reforming over nascent biochar. *Int. J. Hydrogen Energy* **2017**, *42*, 21686–21696. [[CrossRef](#)]
22. Feng, D.; Zhao, Y.; Zhang, Y.; Zhang, Z.; Zhang, L.; Gao, J.; Sun, S. Synergetic effects of biochar structure and AAEM species on reactivity of H<sub>2</sub>O-activated biochar from cyclone air gasification. *Int. J. Hydrogen Energy* **2017**, *42*, 16045–16053. [[CrossRef](#)]
23. Walker, P.L.; Matsumoto, S.; Hanzawa, T.; Muira, T.; Ismail, I.M. Catalysis of gasification of coal-derived cokes and chars. *Fuel* **1983**, *62*, 140–149. [[CrossRef](#)]
24. De Lecea, C.S.-M.; Almela-Alarcón, M.; Linares-Solano, A. Calcium-catalysed carbon gasification in CO<sub>2</sub> and steam. *Fuel* **1990**, *69*, 21–27. [[CrossRef](#)]
25. Feng, D.; Zhao, Y.; Zhang, Y.; Sun, S.; Meng, S.; Guo, Y.; Huang, Y. Effects of K and Ca on reforming of model tar compounds with pyrolysis biochar under H<sub>2</sub>O or CO<sub>2</sub>. *Chem. Eng. J.* **2016**, *306*, 422–432. [[CrossRef](#)]
26. Zhang, Y.; Ashizawa, M.; Kajitani, S.; Miura, K. Proposal of a semi-empirical kinetic model to reconcile with gasification reactivity profiles of biomass chars. *Fuel* **2008**, *87*, 475–481. [[CrossRef](#)]
27. Holstein, W.; Boudart, M. Uncatalyzed and platinum-catalyzed gasification of carbon by water and carbon dioxide. *J. Catal.* **1982**, *75*, 337–353. [[CrossRef](#)]
28. Radovic, L.R.; Walker, P.L.; Jenkins, R.G. Importance of catalyst dispersion in the gasification of lignite chars. *J. Catal.* **1983**, *82*, 382–394. [[CrossRef](#)]
29. Moulijn, J.A.; Cerfontain, M.; Kapteijn, F. Mechanism of the potassium catalysed gasification of carbon in CO<sub>2</sub>. *Fuel* **1984**, *63*, 1043–1047. [[CrossRef](#)]
30. Mims, C.; Pabst, J. Alkali-catalyzed carbon gasification kinetics: Unification of H<sub>2</sub>O, D<sub>2</sub>O, and CO<sub>2</sub> reactivities. *J. Catal.* **1987**, *107*, 209–220. [[CrossRef](#)]
31. Chang, J.-S.; Lauderback, L.L.; Falconer, J.L. AES and SIMS analysis of potassium/graphite surfaces. *Carbon* **1991**, *29*, 645–652. [[CrossRef](#)]
32. Zhao, Y.; Feng, D.; Zhang, Y.; Huang, Y.; Sun, S. Effect of pyrolysis temperature on char structure and chemical speciation of alkali and alkaline earth metallic species in biochar. *Fuel Proc. Technol.* **2016**, *141*, 54–60. [[CrossRef](#)]
33. Andrea Jordan, C.; Akay, G. Speciation and distribution of alkali, alkali earth metals and major ash forming elements during gasification of fuel cane bagasse. *Fuel* **2012**, *91*, 253–263. [[CrossRef](#)]
34. Feng, D.; Zhao, Y.; Zhang, Y.; Sun, S. Effect of speciation of AAEM species on reactivity of biochar. *J. Harbin Inst. Technol.* **2017**, *49*, 69–73.
35. Nutalapati, D.; Gupta, R.; Moghtaderi, B.; Wall, T. Assessing slagging and fouling during biomass combustion: A thermodynamic approach allowing for alkali/ash reactions. *Fuel Proc. Technol.* **2007**, *88*, 1044–1052. [[CrossRef](#)]
36. Miller, S.F.; Miller, B.G. The occurrence of inorganic elements in various biofuels and its effect on ash chemistry and behavior and use in combustion products. *Fuel Proc. Technol.* **2007**, *88*, 1155–1164. [[CrossRef](#)]
37. Benson, S.A.; Holm, P.L. Comparison of inorganic constituents in three low-rank coals. *Ind. Eng. Chem. Prod. Res. Dev.* **1985**, *24*, 145–149. [[CrossRef](#)]
38. Zevenhoven-Onderwater, M.; Backman, R.; Skrifvars, B.-J.; Hupa, M. The ash chemistry in fluidised bed gasification of biomass fuels. Part I: Predicting the chemistry of melting ashes and ash-bed material interaction. *Fuel* **2001**, *80*, 1489–1502. [[CrossRef](#)]
39. Pettersson, A.; Åmand, L.-E.; Steenari, B.-M. Chemical fractionation for the characterisation of fly ashes from co-combustion of biofuels using different methods for alkali reduction. *Fuel* **2009**, *88*, 1758–1772. [[CrossRef](#)]

40. Bai, Y.; Zhu, S.; Luo, K.; Gao, M.; Yan, L.; Li, F. Coal char gasification in H<sub>2</sub>O/CO<sub>2</sub>: Release of alkali and alkaline earth metallic species and their effects on reactivity. *Appl. Therm. Eng.* **2017**, *112*, 156–163. [[CrossRef](#)]
41. Guo, X.; Tay, H.L.; Zhang, S.; Li, C.-Z. Changes in char structure during the gasification of a Victorian brown coal in steam and oxygen at 800 °C. *Energy Fuels* **2008**, *22*, 4034–4038. [[CrossRef](#)]
42. Weng, Q.C.; Wang, C.A.; Che, D.F.; Fu, Z.W. Alkali metal occurrence mode and its influence on combustion characteristics in zhundong coals. *J. Combust. Technol.* **2014**, *20*, 216–221.
43. Feng, D.; Zhang, Y.; Liu, P.; Guo, Y.; Huang, Y.; Sun, S. Effects of chemical fractionation analysis on physical and chemical structures of biomass char. *CIESC J.* **2015**, *66*, 4634–4642.
44. Mitsuoka, K.; Hayashi, S.; Amano, H.; Kayahara, K.; Sasaoaka, E.; Uddin, M.A. Gasification of woody biomass char with CO<sub>2</sub>: The catalytic effects of K and Ca species on char gasification reactivity. *Fuel Proc. Technol.* **2011**, *92*, 26–31. [[CrossRef](#)]
45. Manzoori, A.R.; Agarwal, P.K. The fate of organically bound inorganic elements and sodium chloride during fluidized bed combustion of high sodium, high sulphur low rank coals. *Fuel* **1992**, *71*, 513–522. [[CrossRef](#)]
46. Srinivasachar, S.; Helble, J.; Ham, D.; Domazetis, G. A kinetic description of vapor phase alkali transformations in combustion systems. *Prog. Energy Combust. Sci.* **1990**, *16*, 303–309. [[CrossRef](#)]
47. Marschner, H. *Marschner's Mineral Nutrition of Higher Plants*; Academic Press: Cambridge, MA, USA, 2011.
48. Nordgreen, T.; Liliedahl, T.; Sjöström, K. Metallic iron as a tar breakdown catalyst related to atmospheric, fluidised bed gasification of biomass. *Fuel* **2006**, *85*, 689–694. [[CrossRef](#)]
49. Zhang, S.; Min, Z.; Tay, H.-L.; Asadullah, M.; Li, C.-Z. Effects of volatile–char interactions on the evolution of char structure during the gasification of Victorian brown coal in steam. *Fuel* **2011**, *90*, 1529–1535. [[CrossRef](#)]
50. Tay, H.-L.; Kajitani, S.; Zhang, S.; Li, C.-Z. Effects of gasifying agent on the evolution of char structure during the gasification of Victorian brown coal. *Fuel* **2013**, *103*, 22–28. [[CrossRef](#)]
51. Leites, L.A.; Bukalov, S.S. Raman intensity and conjugation with participation of ordinary  $\sigma$ -bonds. *J. Raman Spectrosc.* **2001**, *32*, 413–424. [[CrossRef](#)]
52. Li, X.; Hayashi, J.; Li, C. Volatilisation and catalytic effects of alkali and alkaline earth metallic species during the pyrolysis and gasification of Victorian brown coal. Part VII. Raman spectroscopic study on the changes in char structure during the catalytic gasification in air. *Fuel* **2006**, *85*, 1509–1517. [[CrossRef](#)]
53. Li, X.; Li, C. Volatilisation and catalytic effects of alkali and alkaline earth metallic species during the pyrolysis and gasification of Victorian brown coal. Part VIII. Catalysis and changes in char structure during gasification in steam. *Fuel* **2006**, *85*, 1518–1525. [[CrossRef](#)]
54. Chen, S.; Yang, R. The Active Surface Species in Alkali-Catalyzed Carbon Gasification: Phenolate (C-O-M) Groups vs Clusters (Particles). *J. Catal.* **1993**, *141*, 102–113. [[CrossRef](#)]
55. Li, C.-Z. Some recent advances in the understanding of the pyrolysis and gasification behaviour of Victorian brown coal. *Fuel* **2007**, *86*, 1664–1683. [[CrossRef](#)]
56. Černý, J. Structural dependence of CH bond absorptivities and consequences for FT-i.r. analysis of coals. *Fuel* **1996**, *75*, 1301–1306. [[CrossRef](#)]
57. Lua, A.C.; Yang, T. Effects of vacuum pyrolysis conditions on the characteristics of activated carbons derived from pistachio-nut shells. *J. Colloid Interface Sci.* **2004**, *276*, 364–372. [[CrossRef](#)] [[PubMed](#)]
58. Lin-Vien, D.; Colthup, N.B.; Fateley, W.G.; Grasselli, J.G. *The Handbook of Infrared and Raman Characteristic Frequencies of Organic Molecules*; Elsevier: Amsterdam, The Netherlands, 1991.
59. Walker, P.; Taylor, R.; Ranish, J. An update on the carbon-oxygen reaction. *Carbon* **1991**, *29*, 411–421. [[CrossRef](#)]
60. Liu, X.; Xu, M.; Yao, H.; Gu, Y.; Si, J.; Xiong, C. Comparison of char structural characteristics and reactivity during conventional air and oxy-fuel combustion. In *Cleaner Combustion and Sustainable World*; Springer: Berlin, Germany, 2013; pp. 989–998.
61. Kelemen, S.; Freund, H. Model CO<sub>2</sub> gasification reactions on uncatalyzed and potassium catalyzed glassy carbon surfaces. *J. Catal.* **1986**, *102*, 80–91. [[CrossRef](#)]
62. Freund, H. Gasification of carbon by CO<sub>2</sub>: A transient kinetics experiment. *Fuel* **1986**, *65*, 63–66. [[CrossRef](#)]
63. Pereira, P.; Csencsits, R.; Somorjai, G.A.; Heinemann, H. Steam gasification of graphite and chars at temperatures <1000 K over potassium-calcium-oxide catalysts. *J. Catal.* **1990**, *123*, 463–476.
64. Kapteijn, F.; Peer, O.; Moulijn, J.A. Kinetics of the alkali carbonate catalysed gasification of carbon: 1. CO<sub>2</sub> gasification. *Fuel* **1986**, *65*, 1371–1376. [[CrossRef](#)]
65. Freund, H. Kinetics of carbon gasification by CO<sub>2</sub>. *Fuel* **1985**, *64*, 657–660. [[CrossRef](#)]

66. Quyn, D.M.; Wu, H.; Hayashi, J.-I.; Li, C.-Z. Volatilisation and catalytic effects of alkali and alkaline earth metallic species during the pyrolysis and gasification of Victorian brown coal. Part IV. Catalytic effects of NaCl and ion-exchangeable Na in coal on char reactivity. *Fuel* **2003**, *82*, 587–593. [[CrossRef](#)]
67. Yu, J.; Tian, F.-J.; Chow, M.C.; McKenzie, L.J.; Li, C.-Z. Effect of iron on the gasification of Victorian brown coal with steam: Enhancement of hydrogen production. *Fuel* **2006**, *85*, 127–133. [[CrossRef](#)]
68. Li, C.-Z.; Sathe, C.; Kershaw, J.; Pang, Y. Fates and roles of alkali and alkaline earth metals during the pyrolysis of a Victorian brown coal. *Fuel* **2000**, *79*, 427–438. [[CrossRef](#)]



© 2018 by the authors. Licensee MDPI, Basel, Switzerland. This article is an open access article distributed under the terms and conditions of the Creative Commons Attribution (CC BY) license (<http://creativecommons.org/licenses/by/4.0/>).